

Cell Biology:

Artesunate Activates Mitochondrial Apoptosis in Breast Cancer Cells via Iron-catalyzed Lysosomal Reactive Oxygen Species Production

Anne Hamacher-Brady, Henning A. Stein, Simon Turschner, Ina Toegel, Rodrigo Mora, Nina Jennewein, Thomas Efferth, Roland Eils and Nathan R. Brady

J. Biol. Chem. 2011, 286:6587-6601.

doi: 10.1074/jbc.M110.210047 originally published online December 13, 2010



Access the most updated version of this article at doi: [10.1074/jbc.M110.210047](https://doi.org/10.1074/jbc.M110.210047)

Find articles, minireviews, Reflections and Classics on similar topics on the [JBC Affinity Sites](https://www.jbc.org/affinity-sites).

Alerts:

- [When this article is cited](#)
- [When a correction for this article is posted](#)

[Click here](#) to choose from all of JBC's e-mail alerts

This article cites 77 references, 30 of which can be accessed free at <http://www.jbc.org/content/286/8/6587.full.html#ref-list-1>

Artesunate Activates Mitochondrial Apoptosis in Breast Cancer Cells via Iron-catalyzed Lysosomal Reactive Oxygen Species Production*

Received for publication, December 8, 2010. Published, JBC Papers in Press, December 13, 2010, DOI 10.1074/jbc.M110.210047

Anne Hamacher-Brady^{‡§¶}, Henning A. Stein^{¶||}, Simon Turschner[‡], Ina Toegel[§], Rodrigo Mora^{¶¶}, Nina Jennewein[§], Thomas Efferth^{**}, Roland Eils^{‡§1}, and Nathan R. Brady^{‡¶||2}

From the [‡]Division of Theoretical Bioinformatics, Applied Systems Biology Group, German Cancer Research Center, 69120 Heidelberg, Germany, the [§]Institute of Pharmacy and Molecular Biotechnology, BioQuant Center, University of Heidelberg, 69120 Heidelberg, Germany, the ^{**}Department of Pharmaceutical Biology, Institute of Pharmacy, University of Mainz, 55128 Mainz, Germany, the [¶]Systems Biology of Cell Death Mechanisms, German Cancer Research Center, 69120 Heidelberg, Germany, and the ^{||}Department of Surgery, Medical Faculty, University of Heidelberg, 69120 Heidelberg, Germany

The antimalarial agent artesunate (ART) activates programmed cell death (PCD) in cancer cells in a manner dependent on the presence of iron and the generation of reactive oxygen species. In malaria parasites, ART cytotoxicity originates from interactions with heme-derived iron within the food vacuole. The analogous digestive compartment of mammalian cells, the lysosome, similarly contains high levels of redox-active iron and in response to specific stimuli can initiate mitochondrial apoptosis. We thus investigated the role of lysosomes in ART-induced PCD and determined that in MCF-7 breast cancer cells ART activates lysosome-dependent mitochondrial outer membrane permeabilization. ART impacted endolysosomal and autophagosomal compartments, inhibiting autophagosome turnover and causing perinuclear clustering of autophagosomes, early and late endosomes, and lysosomes. Lysosomal iron chelation blocked all measured parameters of ART-induced PCD, whereas lysosomal iron loading enhanced death, thus identifying lysosomal iron as the lethal source of reactive oxygen species upstream of mitochondrial outer membrane permeabilization. Moreover, lysosomal inhibitors chloroquine and bafilomycin A1 reduced ART-activated PCD, evidencing a requirement for lysosomal function during PCD signaling. ART killing did not involve activation of the BH3-only protein, Bid, yet ART enhanced TNF-mediated Bid cleavage. We additionally demonstrated the lysosomal PCD pathway in T47D and MDA-MB-231 breast cancer cells. Importantly, non-tumorigenic MCF-10A cells resisted ART-induced PCD. Together, our data suggest that ART triggers PCD via engagement of distinct, interconnected PCD pathways, with hierarchical signaling from lysosomes to mitochondria, suggesting a potential clinical use of ART for targeting lysosomes in cancer treatment.

Artemisinin, the active principle of the Chinese medicinal herb *Artemisia annua* L., and its water-soluble derivative, artesunate (ART),³ are potent antimalarial treatments (1). Additionally, these compounds selectively activate programmed cell death (PCD) in cancer cells (2–4) and inhibit angiogenesis in both *in vitro* and *in vivo* models (7). Importantly, preliminary *in vivo* investigations indicate a therapeutic potential for cancer treatment (5–7), and clinical studies have already shown an excellent safety record in malaria treatment (8). Successful compassionate use of ART in uveal melanoma patients indicates its potential for cancer therapy (9). Components of canonical PCD pathways have been implicated in ART-activated cell death, including p53 (10), Bcl2 family-mediated mitochondrial dysfunction (10, 11), and enhanced reactive oxygen species (ROS) production (12–14). However, detailed understanding of the molecular mechanisms and the sequence of events during ART-induced cell death in cancer cells is limited.

The malaria parasite digests iron-rich hemoglobin in its acidic food vacuole, and the interaction of ART with heme-derived iron results in lethal ROS generation (15). The parasite food vacuole is analogous to eukaryotic lysosomes, organelles that constitute a major site of intracellular degradation via hydrolytic enzymes. Lysosomes are responsible for the degradation of proteins that have been endocytosed and trafficked through the endosomal compartment, as well as for the degradation of cytosolic long- and short-lived proteins and organelles that have entered the lysosome via autophagy pathways (16). Furthermore, endosomes and lysosomes are important sources of redox-active free iron, critical for intracellular biochemistry. Iron release can occur via lysosomal uptake and degradation of cytosolic ferritin (17) and via endocytosed transferrin, which releases iron in the acidic en-

* This work was supported by SBCancer within the Helmholtz Alliance on Systems Biology, funded by the Initiative and Networking Fund of the Helmholtz Association.

¹ Supported by the Bundesministerium für Bildung und Forschung (BMBF)-funded ForSys Centre Viroquant. To whom correspondence may be addressed. E-mail: r.eils@dkfz.de.

² Supported by a fellowship from the ENDOCYTE Marie Curie Research Training Network. To whom correspondence may be addressed. E-mail: n.brady@dkfz.de.

³ The abbreviations used are: ART, artesunate; AV, autophagosomal vesicle; BAF, bafilomycin A1; bis-Tris, 2-[bis(2-hydroxyethyl)amino]-2-(hydroxymethyl)propane-1,3-diol; CQ, chloroquine; DFO, deferoxamine mesylate; FM, full medium; H₂DCF-DA, dichlorodihydrofluorescein diacetate; HTF, diferric holotransferrin; KHS, Krebs-Henseleit solution; LTR, LysoTracker Red; MOMP, mitochondrial outer membrane permeabilization; MR, (z-RR)₂-MagicRed-cathepsin B substrate; PCD, programmed cell death; PepA, pepstatin A; PI, propidium iodide; ROS, reactive oxygen species; TX, trolox.

Artesunate Triggers Lysosomal Cell Death

dosomes (reviewed in Ref. 18). The endolysosomal free iron pool is sensitive and responsive to oxidative stress (19), with hydrogen peroxide reacting with iron to form the reactive hydroxyl radical in a Fenton-type reaction.

Lysosomal ROS generation can cause lysosomal membrane permeabilization (20), whereby lysosomal cathepsins, as well as other hydrolytic enzymes, are released from the lysosomal lumen to the cytosol, and can trigger PCD (21). In the cytosol, lysosomal cathepsins can cleave to activate pro-apoptotic proteins, including Bid (22, 23) and caspase 8 (24), thereby engaging apoptosis through activation of mitochondrial outer membrane permeabilization (MOMP). In the study presented here we sought to determine the contributions and connections of endolysosomes and mitochondria during ART-induced PCD in human breast cancer cells.

EXPERIMENTAL PROCEDURES

Reagents—Artesunate was purchased from Saokim Ltd. Trolox, chloroquine, and holotransferrin were purchased from Sigma. Pepstatin A methyl ester, E64D, deferoxamine mesylate, and bafilomycin A1 were purchased from EMD Biosciences. Ceramide was purchased from Biozol. LysoTracker Red, YO-PRO-1, propidium iodide, and H₂DCF-DA were purchased from Invitrogen. (z-RR)₂-MagicRed-cathepsin B substrate was purchased from B-Bridge International Inc. TNF was a kind gift of BASF (Mannheim, Germany).

Construction of Expression Vectors—To generate mCherry-LC3, LC3 coding sequence was amplified from pEGFP-LC3 (25) inserted into pmCherry-C1. Rab5a (DKFZ clone repository, NM_004162) was amplified and inserted into pmCherry-C1 to generate mCherry-Rab5. To generate Bid sensor, mCherry was fused to full-length Bid (obtained from Ortiz-Ferrón *et al.* (26)) at the N terminus, and GFP was fused in-frame to the C terminus of Bid. The caspase 8-insensitive Bid Δ 60 sensor was obtained using site-directed mutagenesis to generate the D60A mutation (27).

Cell Culture—Human breast cancer cell lines MCF-7 (Cell Lines Services, Heidelberg, Germany), T47D, and MDA-MB-231 (Unit of Toxicology and Chemotherapy, German Cancer Research Center) were maintained in full medium (FM), consisting of DMEM (MCF-7) or RPMI (T47D, MDA-MB-231) supplemented with 10% fetal bovine serum, 2 mM L-glutamine, non-essential amino acids (only for MCF-7), 100 units/ml penicillin, 100 units/ml streptomycin, and 0.25 μ g/ml amphotericin B. MCF-10A human breast epithelial cells were cultured in DMEM/F12 medium supplemented with 5% horse serum, 20 ng/ml epithelial growth factor, 0.5 g/ml hydrocortisone, 10 μ g/ml insulin, 100 units/ml penicillin, 100 units/ml streptomycin, and 0.25 μ g/ml amphotericin B. MCF-7 cell lines stably expressing fusion proteins mitoNEET-(1–23)-GFP (28), mCherry-LC3, GFP-Bax (29), mCherry-Rab5, and GFP-Rab7 (30) were generated by growing transfected cells in FM supplemented with 1 mg/ml G418 (Carl Roth GmbH) for 2 weeks, after which single positive colonies were isolated and propagated. For drug treatments, cells were treated at a confluency of 90–100%. Drug incubations were performed in Krebs-Henseleit solution (KHS, in

mm: 110 NaCl, 4.7 KCl, 1.2 KH₂PO₄, 1.25 MgSO₄, 1.2 CaCl₂, 25 NaHCO₃, 15 glucose, and 10 HEPES, pH 7.4).

96-Well Plate Assays—Cells were plated in black clear-bottom 96-well plates (PerkinElmer Life Sciences) for bottom-to-top readings. Cells were treated in duplicate wells with various drug cocktails in KHS and at the indicated time were incubated with fluorescent probes for 0.5–1 h in separate wells for each dye. Exclusion dyes YO-PRO-1 (0.1–1 μ M) and propidium iodide (PI; 1 μ g/ml) were used to monitor early and late stage apoptotic and necrotic cells and late stage apoptotic and necrotic cells, respectively (31). H₂DCF-DA (10 μ M) was used to monitor ROS generation via the fluorescent nature of its oxidized product, dichlorofluorescein (DCF) (32). Dye fluorescence was measured by a Tecan Infinite M200 plate reader (Tecan) at wavelengths according to manufacturer's instructions.

Fluorescence Imaging—Cells were plated in glass-bottom 8-well μ -slides (iBidi). Wide field fluorescence microscopy was performed with a DeltaVision RT microscope system (Applied Precision) equipped with a \times 40 air objective and a \times 60 oil immersion objective, and images were deconvolved to maximize spatial resolution. Confocal microscopy was performed with a Leica SP5 laser scanning confocal microscope (Leica Microsystems) using a \times 40 oil immersion objective. Images shown are maximum projections of Z-stacks of representative cells covering total cellular fluorescence.

Investigation of Endolysosomal Characteristics—To determine lysosomal functional state, cells were loaded with LysoTracker Red (LTR; 5 nM), which selectively labels acidic lysosomes (30), for 1 h at 37 °C after which time live cells were imaged immediately. Cathepsin B activity and localization were analyzed using (z-RR)₂-MagicRed-cathepsin B substrate (MR). MR was reconstituted and incubated at a concentration of 2.2 μ M for 1 h at 37 °C prior to the imaging of live cells. To assess the intracellular distribution of early endosomes, MCF-7 cells stably expressing mCherry-Rab5 were subjected to live cell imaging. Similarly, the intracellular distribution of late endosomes and lysosomes was investigated using MCF-7 cells stably expressing GFP-Rab7 (33). Alternatively, lysosomes were visualized in cells fixed with 4% paraformaldehyde (EMS) by immunostaining with mouse anti-Lamp2a (Santa Cruz Biotechnology)/Alexa Fluor 546 goat anti-mouse (Invitrogen). Z-stacks or two-dimensional images of live or fixed cells were obtained at \times 60 magnification and 1- μ m increments.

Measurement of Events Associated with MOMP—These events were measured as follows. (i) To examine mitochondrial morphology, MCF-7 cells stably expressing the outer mitochondrial marker, mitoNEET-(1–23)-GFP (28), were subjected to the indicated drug treatments. At 24 h, Z-stacks of live cells were taken at \times 60 magnification and 1- μ m increments. Mitochondria were identified as either elongated and networked or as fragmented. (ii) Intracellular GFP-Bax (29) distribution was used to quantify Bax activation. MCF-7 cells stably expressing GFP-Bax were subjected to the indicated conditions. At 24 h, Z-stacks were captured at \times 40 magnification and 1- μ m increments. From maximum projection images, cells were classified as exhibiting either diffuse cytosolic

(inactive) or punctate mitochondrial (active) GFP-Bax fluorescence. (iii) Cytochrome *c* was determined in paraformaldehyde-fixed cells following staining with mouse anti-cytochrome *c* (BD Biosciences)/Alexa Fluor 546 goat anti-mouse (Invitrogen), in combination with rabbit anti-COX IV (Cell Signaling)/Alexa Fluor 488 goat anti-rabbit (Invitrogen), to visualize mitochondria. Nuclei were labeled with Hoechst 33342 (1 $\mu\text{g}/\text{ml}$, Invitrogen). Z-stacks of two fields-of-view/condition were obtained at $\times 40$ magnification and 0.6–1- μm increments. Quantitative analysis was performed using ImageJ (NIH). The total number of cells was determined from manually adjusted, Otsu-thresholded Hoechst channels using the “nucleus counter” plug-in. Cells were then scored as cells with mitochondrial cytochrome *c*, *i.e.* colocalized COX IV and cytochrome *c*, and cells with cytosolic cytochrome *c*, *i.e.* loss of colocalization with COX IV.

Flow Cytometry—MCF-7 cells were plated in 96-well plates and treated for 24 h. After the indicated treatment period, cells were incubated with either LTR (100 nM) or MagicRed (2.2 μM) for 1 h. Detached and trypsinized cells were collected, and flow cytometry was performed with a Beckman Coulter FC500 flow cytometer, custom-equipped with a 561 nm laser. Mean intensity values were normalized to the control cells in KHS.

Western Blotting—Detached and adherent cells were collected, and whole cell lysates were prepared with radioimmuno precipitation assay buffer (Millipore) containing complete protease inhibitor mixture (Roche Applied Science). Protein concentrations were determined using Coomassie reagent (Sigma). Samples were electrophoresed in using either 10% (Bid and GFP (Fig. 8)) or 12% (LC3B (Fig. 3)) bis-Tris NuPAGE (Invitrogen), and proteins were then transferred to nitrocellulose using the iBlot dry blotting system (Invitrogen). Immunodetection was performed using antibodies against β -actin (Abcam), Bid (Cell Signaling), GFP (Cell Signaling), and LC3B (Cell Signaling). LC3 blots were prepared using HRP-linked secondary antibodies (Cell Signaling) and analyzed with an Intas chemiluminescence imager. Bid blots were prepared using fluorescently labeled secondary antibodies, DyLight 680 and DyLight 800 (Thermo Scientific), and analyzed with an Odyssey infrared imaging system (Licor). Blots shown are representative of at least three independent experiments.

Statistical Analyses—Measurements were normalized to control (KHS conditions), and the probability of statistically significant increases or decreases between conditions was determined using the Student's *t* test. One-tailed *t* tests were performed, paired for matched data sets and unpaired for unmatched data sets. Values are expressed as mean \pm S.E. of at least three independent experiments.

RESULTS

ART Activates Cell Death of MCF-7 Breast Cancer Cells

We initially determined the conditions under which ART triggers robust cell death in MCF-7 cells, as a function of concentration and time (Fig. 1A). MCF-7 cells were incubated in Krebs-Henseleit solution (KHS), a defined glucose-containing

basic salt solution, with or without ART at concentrations of 1, 10, and 20 $\mu\text{g}/\text{ml}$, previously shown to be cytotoxic in cancer cells (10). At time points of 24 and 48 h, cell viability was determined by exclusion dyes: YO-PRO-1 to label early and late stage apoptotic cells and necrotic cells, and PI, to label late stage apoptotic and necrotic cells (34). TNF (43 ng/ml), an inflammatory cytokine, was used as a positive control for apoptosis induction, with significant cell death detection at 24 and 48 h. ART concentrations of 10 and 20 $\mu\text{g}/\text{ml}$ significantly activated cell death in a dose-dependent manner after 24 and 48 h of treatment. ART at 1 $\mu\text{g}/\text{ml}$ induced significant levels of cell death only after 48 h.

ROS Are Causative in ART-induced Cell Death

Earlier studies have implicated ROS as an important mediator of ART-induced cell death in cancer cells (35). Therefore, we measured the effect of ART on ROS levels in MCF-7 cells during the early (18 h) cell death-signaling phase using $\text{H}_2\text{DCF-DA}$, a live cell ROS indicator (32). As shown in Fig. 1C, ROS levels significantly increased in ART-treated but not TNF-treated cells. To determine the role of ROS in death signaling, cells were co-treated with trolox (TX), a water-soluble vitamin E analog and potent scavenger of the hydroxyl radical (36). TX abolished ART-induced ROS generation and had no effect on ROS levels in TNF-treated cells (Fig. 1C). Moreover, TX significantly reduced ART-induced cell death at both 24 and 48 h, whereas TX did not affect TNF-induced cell death (Fig. 1B). These data indicate ROS as a causative factor in ART- but not TNF-triggered cell death.

Endolysosomal Iron Chelation Confers Potent Protection from ART-triggered PCD

Redox-active iron in mammalian lysosomes is an important intracellular lethal source of ROS (20). Moreover, iron-derived ROS are a contributing factor in ART-induced cell death in the malaria parasite (15). Therefore, we investigated the role of lysosomal iron in ART-activated ROS production and PCD in MCF-7 cells by employing the iron chelator deferoxamine mesylate (DFO). DFO specifically targets lysosomal iron as it enters the cell via endocytosis and accumulates in the lysosome (37).

DFO (0.1 mM) alone slightly (not significant) increased basal ROS (Fig. 2A, 18 h) and cell death (Fig. 2B, 48 h) levels in both control and TNF-treated cells. In combination with ART, DFO decreased ART-triggered ROS production, with a significant difference for ART at 20 $\mu\text{g}/\text{ml}$. Moreover, at 48 h DFO significantly decreased ART-induced cell death to the levels of DFO alone at ART concentrations of both 10 and 20 $\mu\text{g}/\text{ml}$.

Endolysosomal Iron Loading Enhances ART-triggered PCD

As scavenging lysosomal free iron reduced ART-activated cell death, we sought to determine whether increasing endolysosomal iron could enhance ART-activated cell death. We employed diferric holotransferrin (HTF), which is actively internalized by receptor-mediated endocytosis; during transit through endolysosomes, bound iron is released due to low pH environment (18). HTF at concentrations of 0.05, 0.5, and 5

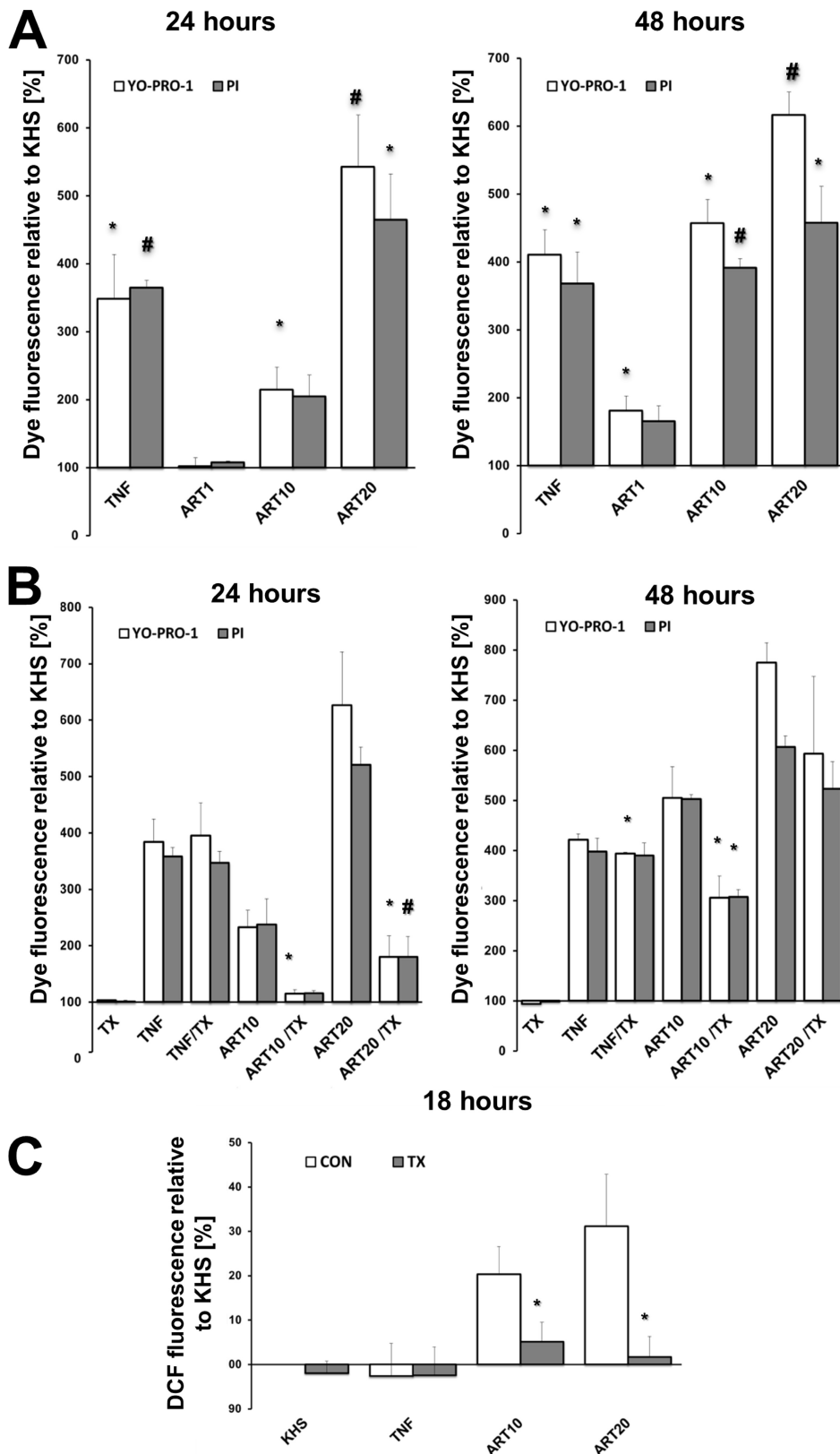


FIGURE 1. ART activates ROS-dependent cell death in MCF-7 cells. A, ART-induced cell death is dose- and time-dependent. MCF-7 cells were either incubated in KHS alone or treated with 1, 10, or 20 $\mu\text{g/ml}$ ART in KHS. Cell death was assessed at 24 and 48 h using exclusion dyes PI (1 $\mu\text{g/ml}$) and YO-PRO-1 (0.1 μM) in a fluorescence plate reader assay. Cell death is represented as the percentage of dye fluorescence normalized to KHS, and the x axis crosses at 100%, i.e. basal KHS levels (*, $p < 0.05$; #, $p < 0.001$, compared with KHS). B, ART-induced PCD is inhibited by the ROS scavenger TX. MCF-7 cells were treated with the indicated drugs in KHS for 24 and 48 h as indicated, and cell death was determined as described in A. (*, $p < 0.05$; #, $p < 0.001$, without TX versus with TX). C, TX blocks ART-induced increase in ROS. MCF-7 cells were subjected to drug treatments with and without TX (0.25 mM). At 18 h ROS production was assessed using $\text{H}_2\text{DCF-DA}$ and graphed normalized to KHS. (*, $p < 0.05$, without TX versus with TX).

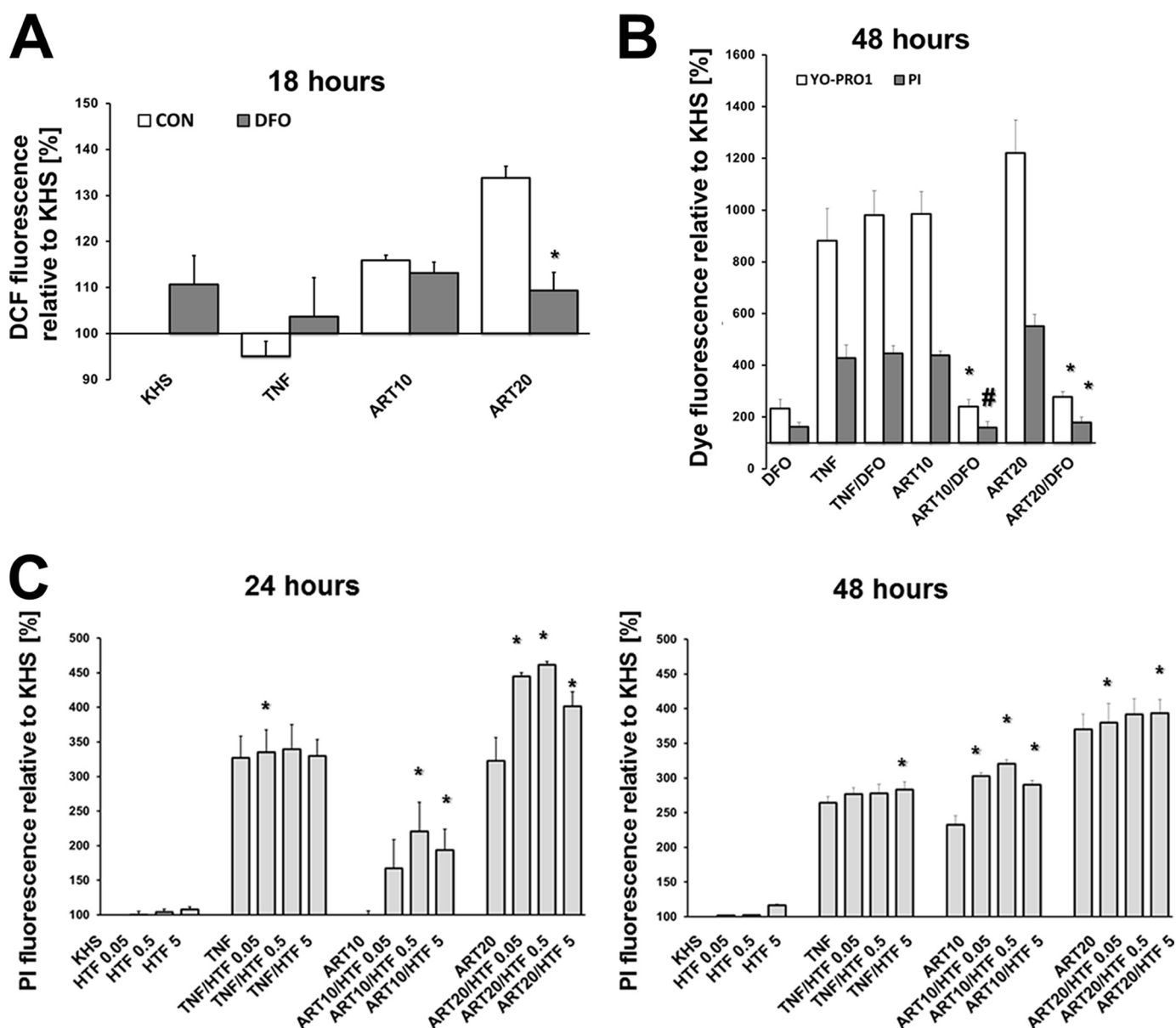


FIGURE 2. **Endolysosomal iron mediates ART-activated PCD signaling.** *A* and *B*, MCF-7 cells were treated with the iron chelator DFO (0.1 mM) and/or the indicated drug in KHS. *A*, ROS generation was determined at 18 h using $H_2DCF\text{-}DA$ ($10\ \mu M$) (*, $p < 0.05$; without DFO versus with DFO). *B*, cell death was measured at 48 h using YO-PRO-1 ($1\ \mu M$) and PI ($1\ \mu g/ml$) (*, $p < 0.05$; #, $p < 0.001$, without DFO versus with DFO). The percentage of dye fluorescence normalized to KHS is graphed. The x axis crosses at 100% (i.e. KHS), signifying basal ROS (*A*) or cell death (*B*) levels. *C*, endolysosomal iron content was increased via incubation with diferric HTF (0.05, 0.5, and $5\ \mu M$). Cell death was measured at 24 and 48 h using PI ($1\ \mu g/ml$). Graphs indicate responses as the percentage of dye fluorescence normalized to KHS, and the x axis crosses at 100%, i.e. basal KHS levels (*, $p < 0.05$, with HTF versus without HTF).

μM alone had no impact on cell viability, and HTF did not impact TNF-induced cell death. HTF co-treatment with both 10 and 20 $\mu g/ml$ ART significantly increased cell death at 24 h and at 48 h (Fig. 2C). The ensemble of findings given above indicates that lysosomal free iron serves as the major source of ROS and thereby is a critical prerequisite during ART-mediated cell death in MCF-7 breast cancer cells.

Impact of ART on Autophagosomal/Endolysosomal Activity

Both DFO and HTF accumulate in endolysosomes, and as such their respective antagonizing and enhancing effects on ART-activated cell death suggest a pro-death role for the endolysosomal compartment. To that end we determined the

impact of ART on several parameters of lysosomal function, including autophagy, endolysosomal trafficking, and lysosomal activity state at population, single cell, and subcellular levels.

ART Inhibits Autophagosome Turnover—The impact of ART on autophagy was investigated in MCF-7 cells stably expressing mCherry-LC3, which labels both autophagosomes and autolysosomes (38), referred to here as autophagosomal vesicles (AVs). Under FM conditions, where basal autophagic activity is low, numerous small AVs were distributed homogeneously throughout the cell. Under KHS conditions, where autophagy is up-regulated, increased levels of AVs were detected, likely corresponding to autolysosomes, and these were

Artesunate Triggers Lysosomal Cell Death

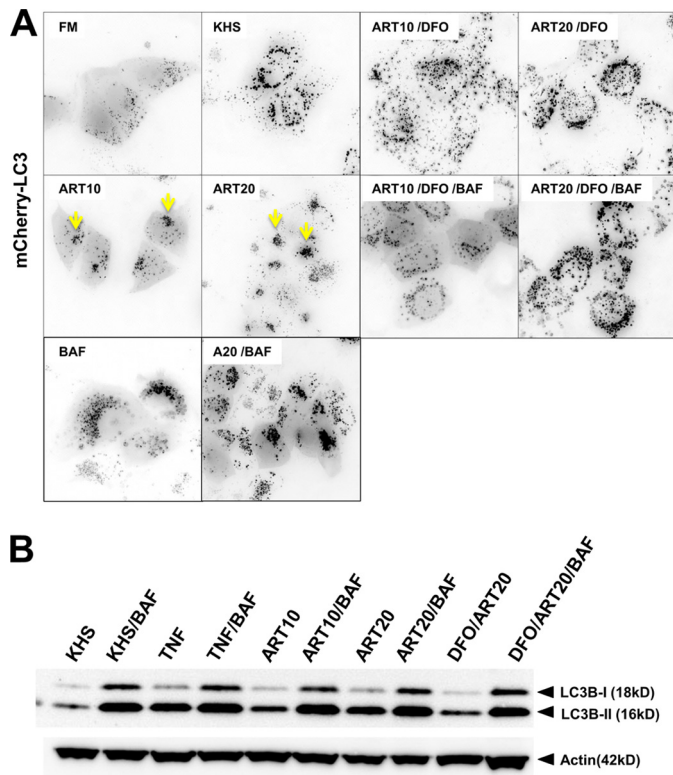


FIGURE 3. ART inhibits turnover of AVs and induces perinuclear AV clustering. *A*, MCF-7 cells stably expressing mCherry-LC3 were subjected to the indicated conditions for 24 h. Autophagic flux was inferred by comparing cellular AV content and localization in the absence (steady-state AVs) and presence (cumulative AVs) of lysosomal inhibitor BAF (100 nM, 3 h of treatment). *B*, Western blot analysis of cytosolic LC3B-I (~18 kDa) and membrane-bound LC3B-II (~16 kDa) abundance in the absence and presence of BAF.

dispersed throughout the cell. In response to both ART 10 $\mu\text{g/ml}$ and ART 20 $\mu\text{g/ml}$, AVs were clustered to the perinuclear region (Fig. 3*A*, arrows). DFO treatment prevented AV clustering in response to ART.

At any given time, the number of steady-state autophagosomes is a function of autophagosome formation and degradation, *i.e.* flux. To determine autophagic flux, it is necessary to compare the number of steady-state AVs with the number of AVs accumulating in the presence of lysosomal protease inhibitors, *i.e.* AV formation in the absence of degradation (38, 39). Here, lysosomal activity was inhibited using 0.1 μM bafilomycin A1 (BAF), which through inhibition of the lysosomal V-ATPase raises lysosomal pH and consequently decreases cathepsin activities (40). As expected, under KHS conditions both the number and size of AVs increased considerably within BAF-treated cells (Fig. 3*A*). Similarly, in ART-treated cells, BAF induced an increase in AVs, but AVs remained clustered. Cells that were treated with ART in the presence of DFO displayed active autophagic flux, similar to the observed accumulation of AVs in KHS in the presence of BAF. Furthermore, DFO reversed ART-induced clustering of AVs. These data indicate that, dependent on lysosomal iron, (i) ART blocks AV degradation, as formed AVs accumulated under steady-state conditions, whereas cumulative levels of AVs showed no apparent effect; and (ii) ART spatially dis-

rupts autophagy, as AVs were clustered to perinuclear regions.

To confirm the inhibitory effect of ART on autophagy, Western blot analysis was performed to detect changes in abundance of cytosolic LC3B-I (~18 kDa) and autophagosomal LC3B-II (~16 kDa). Cells were treated for 18 h followed by the addition of BAF for 3 h to block LC3B-II degradation (Fig. 3*B*). Under KHS conditions, low levels of steady-state LC3B-I and LC3B-II were detected. In response to BAF both LC3B-I and LC3B-II increased, indicating the level of active flux during nutrient deprivation. TNF treatment resulted in higher levels of steady-state LC3B-I and LC3B-II, with cumulative levels similar to KHS, indicating a reduction to both LC3B-I to II conversion and a block in LC3B-II degradation. Similarly, steady-state LC3B-II levels were increased in response to ART 10 $\mu\text{g/ml}$ and were more pronounced in response to ART 20 $\mu\text{g/ml}$ compared with KHS, indicating that ART reduced autophagic flux in a concentration-dependent manner. As observed in imaging experiments, DFO reversed the block to autophagic flux, thus implicating lysosomal iron as a causative factor.

ART Disruption of Endolysosomal Trafficking Is Dependent on Lysosomal Iron—The above results suggested a disruption to the endolysosomal system, which operates in parallel and in conjunction with autophagy (41). Rab proteins, a family of small GTPases, control endosome trafficking, interactions, and function (42). We therefore determined the intracellular distribution of Rab5, a GTPase recruited to the early endosome and critical component of endocytosis (43), and Rab7, which is acquired in late endosomes and controls the fusion of autophagosomes and endosomes with the lysosome (30).

In MCF-7 cells stably expressing either mCherry-Rab5 or GFP-Rab7 we determined the impact of ART at 24 h of treatment (Fig. 4). Under FM conditions both Rab5- and Rab7-labeled vesicles were dispersed throughout the cytosol, and under KHS conditions the number and size of labeled vesicles increased while their distribution remained unchanged. TNF-treated cells showed no difference in either mCherry-Rab5 or GFP-Rab7 distribution compared with the KHS condition. In contrast, in a dose-dependent manner, ART 10 $\mu\text{g/ml}$ and ART 20 $\mu\text{g/ml}$ treatment resulted in the asymmetric clustering of the majority of both early and late endosomes to the perinuclear region. DFO blocked ART-induced clustering of Rab5- and Rab7-labeled vesicles, similar to the blocking effect of DFO on ART-induced clustering of mCherry-LC3-labeled AVs (Fig. 3*A*).

ART Does Not Impact Total Cellular Lysosomal pH and Cathepsin B Activity—We subsequently determined whether vesicular clustering correlated with perturbed lysosomal function. LysoTracker Red (LTR), which labels acidic compartments in live cells, was used to assess activity of the V-ATPase, which acidifies the lysosomal lumen to maintain full activity of cathepsin proteases (40). To compare the lysosomal effects of ART with reported initiators of lysosomal dysfunction, we employed the V-ATPase inhibitor BAF (0.1 μM) and the lysosomotropic compound chloroquine (CQ; 30 μM) (Fig. 5*C*). Experiments were performed in wild-type MCF-7 cells at 24 h of treatment. Under FM conditions, cells

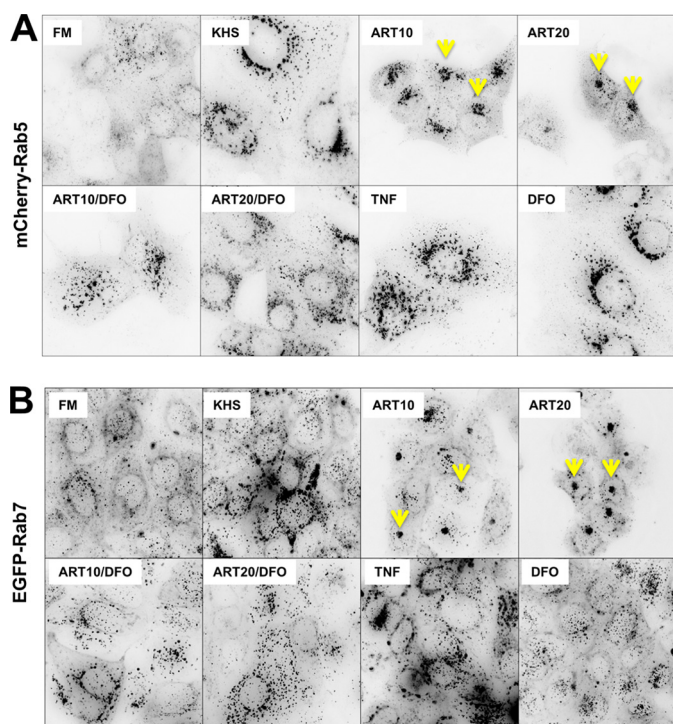


FIGURE 4. ART induces perinuclear clustering of early endosomes, late endosomes, and lysosomes. *A*, at 24 h of indicated drug treatments, abundance and intracellular distribution of early endosomes were investigated in MCF-7 cells stably expressing mCherry-Rab5. *B*, abundance and intracellular distribution of late endosomes and lysosomes were investigated in MCF-7 cells stably expressing GFP-Rab7 at 24 h of indicated drug treatments.

displayed numerous small LTR-positive vesicles (Fig. 5A). Under KHS conditions, LTR-labeled vesicles increased in size, number, and LTR intensity. Inhibition of lysosomal activity using BAF resulted in complete absence of LTR labeling. CQ resulted in enhanced vesicle size and LTR intensity, consistent with previously reported CQ-induced increase in lysosomal activities (44, 45). TNF-treated cells showed no difference in LTR signal compared with the KHS control. ART, at both 10 and 20 $\mu\text{g}/\text{ml}$, resulted in an LTR signal detectable only in perinuclear clusters. Treatment with DFO (0.1 mM) alone had no impact on LTR staining (Fig. 5C). In combination with ART (10 and 20 $\mu\text{g}/\text{ml}$), DFO blocked the clustering of LTR-positive vesicles, and the number and cytosolic localization of LTR-positive vesicles were comparable to those of the KHS control.

As a second parameter of lysosomal function, we examined the activity of the prominent lysosomal protease cathepsin B using MR. MCF-7 cells stably expressing GFP-Rab7 were subjected to 24 h of drug treatments. Similar to LTR, cells kept in FM displayed numerous small MR-positive vesicles, which co-localized fully with GFP-Rab7 (results not shown). Under KHS conditions, the number and size of MR- and GFP-Rab7-positive vesicles increased (Fig. 5B). Treatment with BAF (0.1 μM) resulted in reduced MR fluorescence, and similar to LTR results, CQ (30 μM) enhanced the size and labeling by MR (Fig. 5C). Incubation with ART (10 and 20 $\mu\text{g}/\text{ml}$) resulted in MR/Rab7-GFP-positive vesicles clustering to the perinuclear region (Fig. 5B). DFO alone had no effect, but in combination

with ART (as opposed to ART alone), the number and cytosolic localization were comparable with those of the KHS control. Flow cytometry was performed to quantify the effects of ART on pH and cathepsin activity. Consistent with imaging results, BAF reduced and CQ increased the mean fluorescence levels of LTR and MR. ART had no significant impact on the mean fluorescence levels of LTR and MR, indicating that although ART altered the localization of endolysosomes, the acidity state and protease activity were not impacted (Fig. 5D).

ART Signaling Requires an Initially Functional Lysosomal Compartment

The above results indicate that ART induces functional (*i.e.* ROS generation) and spatial (*i.e.* clustering) alterations to the endolysosomal compartment. As such, we determined whether additional targeting of lysosomes by combinatorial treatment of ART with lysosomal inhibitors would augment ART-induced PCD. TNF was included as a reference, as it did not impact the measured parameters of endolysosomal activity or trafficking during PCD signaling (Fig. 5). Wild-type MCF-7 cells were treated with either 20 $\mu\text{g}/\text{ml}$ ART or TNF alone or in combination with BAF or CQ for 18 h. Both BAF and CQ significantly decreased ART-induced ROS levels (Fig. 6A), yet neither had a significant impact on ROS production when combined with TNF. At 18 h of treatment, both BAF and CQ co-treatments reduced ART-induced PCD while significantly increasing cell death in combination with TNF (Fig. 6B). ART-induced levels of cell death were most potently reduced by BAF, which reduced cell death to levels comparable with treatment with BAF alone. Together, these data suggest that ART-mediated PCD signaling requires the initial participation of functional lysosomes.

ART Activates Lysosomal Iron-dependent MOMP

Lysosomal dysfunction can activate mitochondrial apoptosis (45, 46), and previous work determined that ART activates cell death via mitochondrial apoptosis (35). To investigate the relationship between ART-activated lysosomal dysfunction and apoptosis, multiple parameters of mitochondrial dysfunction were determined.

ART Triggers Lysosomal Iron-dependent Mitochondrial Fragmentation—Under normal conditions mitochondria exist as a dynamic network that is controlled by a balance between mitochondrial fission and fusion events (47). During mitochondrial apoptosis, the machinery controlling fragmentation participates in MOMP (29). To assess the participation of mitochondria in ART-triggered cell death in MCF-7 breast cancer cells, mitochondrial morphology was determined in MCF-7 cells stably expressing a GFP tag at the outer mitochondrial membrane (28).

At 24 h, under FM and KHS conditions, mitochondria were distributed throughout the cell and exhibited a highly networked morphology (Fig. 7A). DFO-treated cells displayed a phenotype similar to control cells. In ART-treated cells (10 and 20 $\mu\text{g}/\text{ml}$), mitochondria were also distributed throughout the cell, but mitochondrial networks were fully fragmented. Remarkably, cells treated with ART (10 and 20 $\mu\text{g}/$

Artesunate Triggers Lysosomal Cell Death

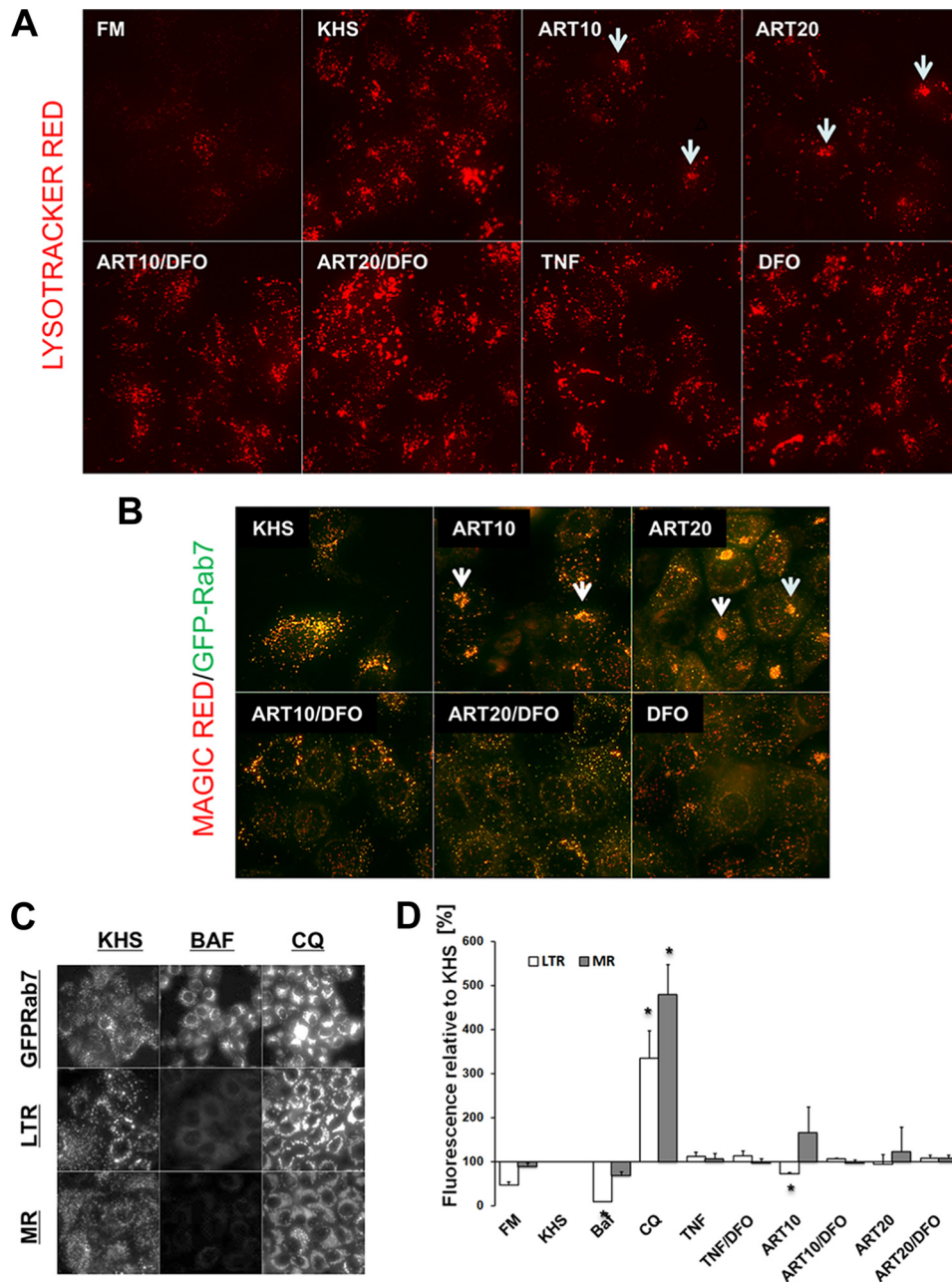


FIGURE 5. ART disrupts localization of endolysosomes but not apparent function of critical lysosomal parameters. *A*, wild-type MCF-7 cells were subjected to the indicated experimental conditions for 24 h and then labeled with the lysosomal pH indicator LTR (5 nM) and analyzed by fluorescence microscopy. *B*, MCF-7 cells stably expressing GFP-Rab7 were incubated with MR cathepsin B substrate (2.2 μ M) following 24 h of drug treatments. Both GFP-Rab7 and MR were analyzed by fluorescence microscopy. *C*, Rab7, LTR, and MR staining and intensity patterns were analyzed in MCF-7 wild-type cells (*LTR*) and cells stably expressing GFP-Rab7 (*Rab7* and *MR*) following 3 h of treatment. *D*, flow cytometry was used to quantify population level responses. The mean fluorescence intensity of lysosomal LTR (0.1 μ M) and MR (2.2 μ M) was determined. Graphs indicate responses as the percentage of dye fluorescence normalized to KHS, and the x axis crosses at 100% (*, $p < 0.05$; #, $p < 0.001$, compared with KHS).

ml) in the presence of DFO displayed the highly networked mitochondrial phenotype of control cells. In TNF-treated cells, mitochondria were localized to the perinuclear region and exhibited a fragmented and swollen phenotype. DFO had no inhibitory effect on TNF-induced mitochondrial fragmentation or swelling.

ART Triggers Iron-dependent Bax Clustering—In response to apoptotic stimuli, Bax, a multidomain pro-apoptotic member of the Bcl-2 family, translocates from the cytosol to the mitochondria where it induces MOMP (29). Upon activation

at the mitochondria, Bax forms high molecular weight aggregates at mitochondrial fission sites, considered the key event for cytochrome *c* release (29). At 24 h, under KHS conditions, GFP-Bax was distributed homogeneously in the majority of control cells (Fig. 7, *Bi* and *Bii*). In response to TNF, the majority of cells displayed clustered (*i.e.* active) GFP-Bax. ART induced a dose-dependent increase in GFP-Bax clustering that was significantly reduced by DFO. Notably, DFO had no protective effect on GFP-Bax clustering in TNF-treated cells.

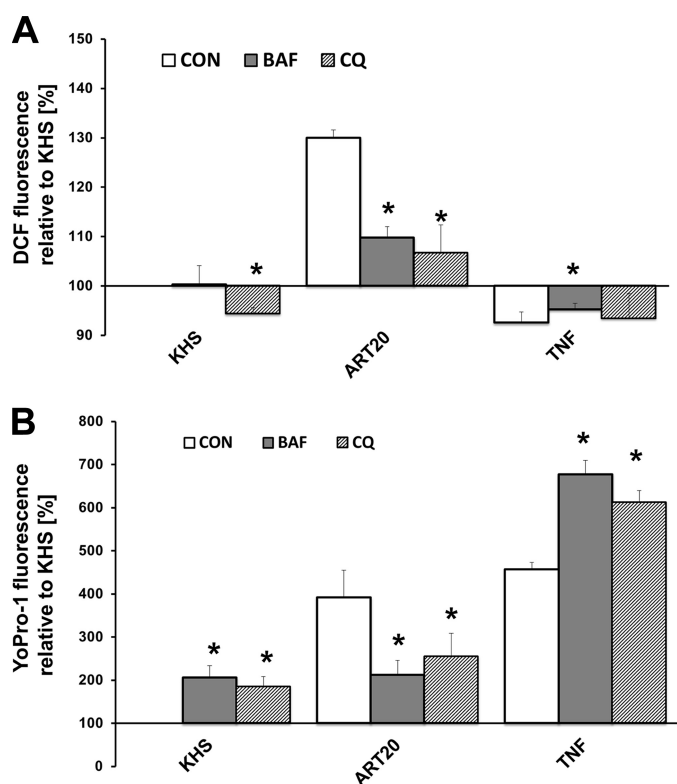


FIGURE 6. ART-induced PCD is dependent on lysosomal function. Co-treatments with lysosomal perturbators BAF (0.1 μM) and CQ (30 μM) and either ART or TNF were performed in wild-type MCF-7 cells *A*, ROS generation was determined at 18 h using $\text{H}_2\text{DCF-DA}$ (10 μM). *B*, cell death was measured at 18 h using YO-PRO-1 (0.1 μM). Graphs indicate responses as the percentage of dye fluorescence normalized to KHS, and the x axis crosses at 100%, i.e. basal KHS levels (*, $p < 0.05$; #, $p < 0.001$, without versus with co-treatments).

Cytochrome *c* Release by ART Is Iron-dependent—The release of cytochrome *c* was determined at 48 h by high-resolution imaging of cytochrome *c* and COX IV immunostaining in wild-type MCF-7 cells (Fig. 8C). Treatment with TNF served as a positive control for the activation of cytochrome *c* release. In ART-treated cells the percentage of cells displaying cytochrome *c* release was significantly increased compared with the control. DFO in combination with ART reduced cytochrome *c* release to levels comparable with that in DFO alone, significantly so in ART 20 $\mu\text{g/ml}$ -treated cells. In contrast, DFO slightly enhanced TNF-induced cytochrome *c* release, consistent with cell death measurements (Fig. 2B).

Together, these data evidence a signaling pathway whereby iron-dependent lysosomal dysfunction induces classical parameters of mitochondrial apoptosis, including mitochondrial fragmentation, Bax activation, and cytochrome *c* release during ART-triggered cell death.

BH3-only Protein Bid and Cathepsins D, B, and L Do Not Participate in the Lysosome-to-Mitochondria Transmission of ART Death Signaling

Lysosomes can trigger mitochondrial apoptosis via cathepsin-mediated Bid cleavage (23, 48). To detect Bid cleavage we employed a derivative of an established fluorescent protein-based Bid biosensor (49), here with an N terminus mCherry and C terminus GFP tags (mCherry-Bid-GFP). Bid cleavage to

active tBid was determined by Western blotting in MCF-7 cells stably expressing mCherry-Bid-GFP. Under control KHS conditions, the Bid sensor was detected as a triplet band at around the predicted size of 76 kDa. The multiple band migration pattern was also detected when expressing the mCherry-GFP fusion protein and was therefore due to the presence of mCherry (results not shown).

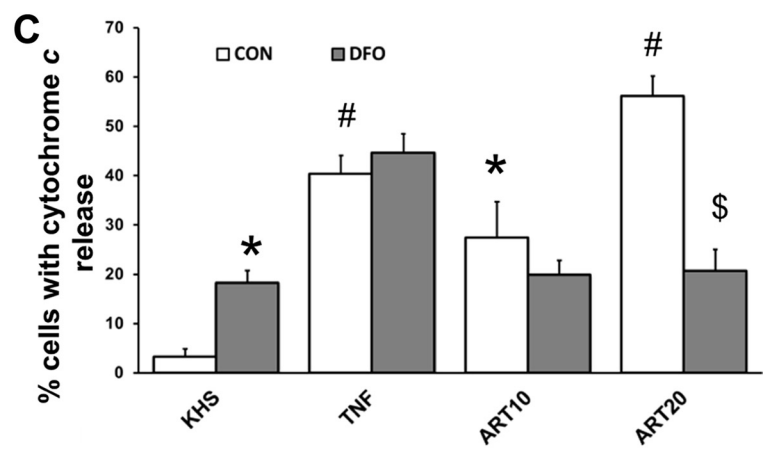
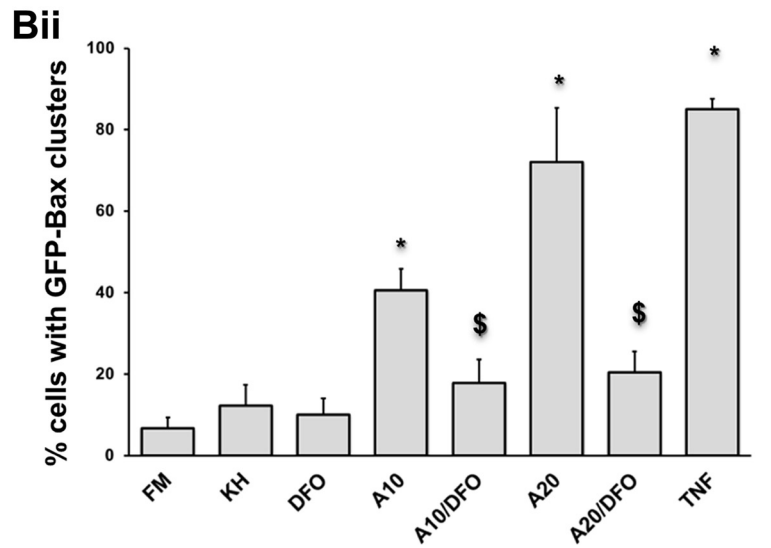
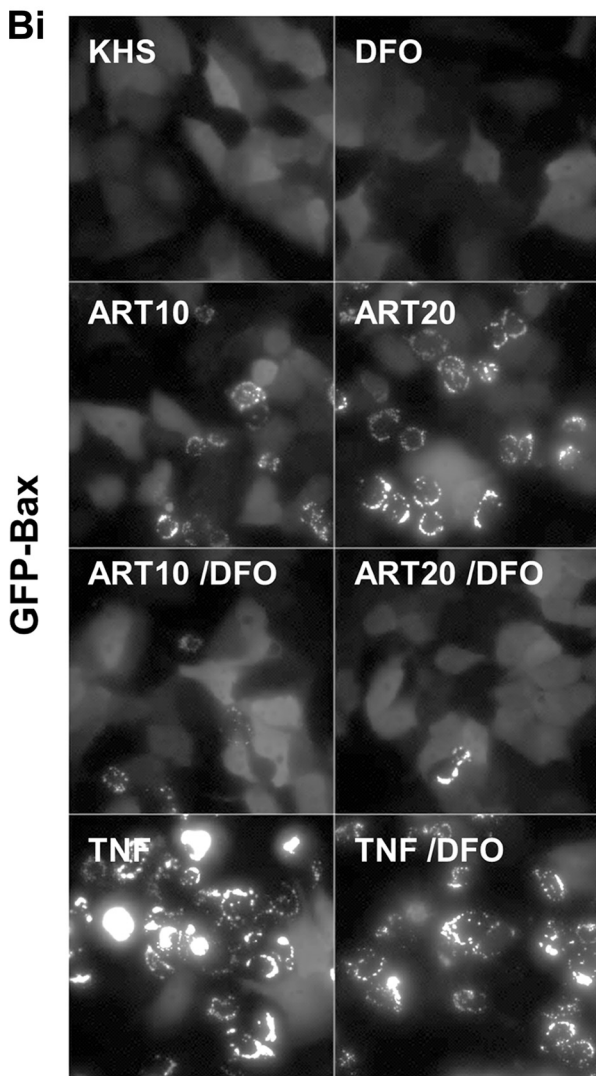
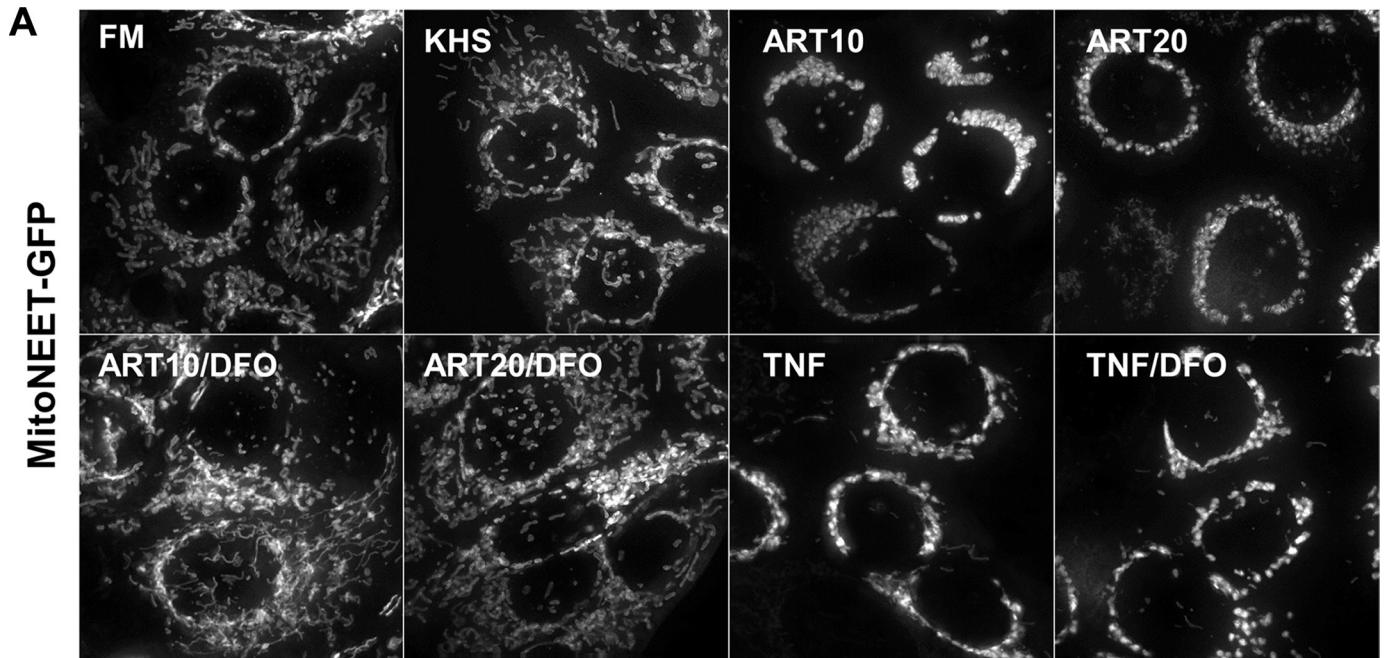
In response to TNF, a single major cleavage product at 42 kDa was detected by GFP antibodies corresponding to tBid-GFP (predicted 42.5 kDa), and the appearance of tBid-GFP coincided with loss of endogenous Bid. At 24 h no Bid cleavage occurred in response to ART at either 10 or 20 $\mu\text{g/ml}$. Interestingly, co-treatment with ART resulted in enhanced TNF-induced cleavage of Bid sensor and clearance of endogenous Bid (Fig. 8A, left). To identify the protease responsible for Bid cleavage during combined TNF/ART treatment (e.g. caspase, calpain, or cathepsin), a D60A substitution was inserted at the major caspases 8 and 2 cleavage sites (50), referred to here as Bid Δ 60 sensor. As such, Bid Δ 60 sensor cannot be cleaved by caspases 8 and 2 but can still be cleaved by cathepsin and calpain proteases (51). As expected, no cleavage of Bid Δ 60 sensor was detected in response to TNF or ART treatment alone, and endogenous Bid clearance was similar to that detected in wild-type Bid sensor cells. Likewise, no cleavage was detected with TNF and either ART 10 $\mu\text{g/ml}$ or ART 20 $\mu\text{g/ml}$ co-treatments (Fig. 8A, right).

We then addressed the participation of cathepsins by measuring ART-induced cell death in the presence of the specific cathepsin D inhibitor, pepstatin A (PepA; 5 $\mu\text{g/ml}$) and the cathepsin B/L inhibitor EST (10 $\mu\text{g/ml}$) (Fig. 8B). PepA/EST enhanced both TNF killing and ART-induced cell death, indicating that cathepsins are not initiators of MOMP.

ART Specifically Triggers Lysosomal Iron-dependent PCD Also in Caspase 3-positive Breast Cancer Cells but Not in Non-transformed Breast Epithelial Cells

To investigate the significance of the lysosomal PCD pathway described above, we determined the effects of ART in T47D breast cancer cells, which like MCF-7 cells are estrogen receptor-positive, and MDA-MB-231 breast cancer cells, which are estrogen receptor-negative (52). In addition, MCF-10A breast epithelial cells, which are immortalized but non-transformed, were utilized as a non-cancer cell type. Importantly, unlike MCF-7 cells, all additional cell lines express caspase 3 (53).

At 48 h of treatment, cell death was determined (Fig. 9Ai). In T47D cells, TNF had no impact and ART was slightly toxic only at 20 $\mu\text{g/ml}$. HTF alone had no impact on cell viability, but HTF in combination with ART (10 and 20 $\mu\text{g/ml}$) resulted in significant, ART dose-dependent killing. Importantly, this effect was blocked by the addition of either DFO or TX. In MDA-MB-231 cells TNF slightly but insignificantly enhanced cell death. ART (10 and 20 $\mu\text{g/ml}$) treatment alone resulted in significant, dose-dependent killing. Similar to T47D cells, HTF co-treatment significantly enhanced ART-induced cell killing. Also in MDA-MB-231 cells, HTF-enhanced ART-mediated cell death was blocked by DFO and TX.



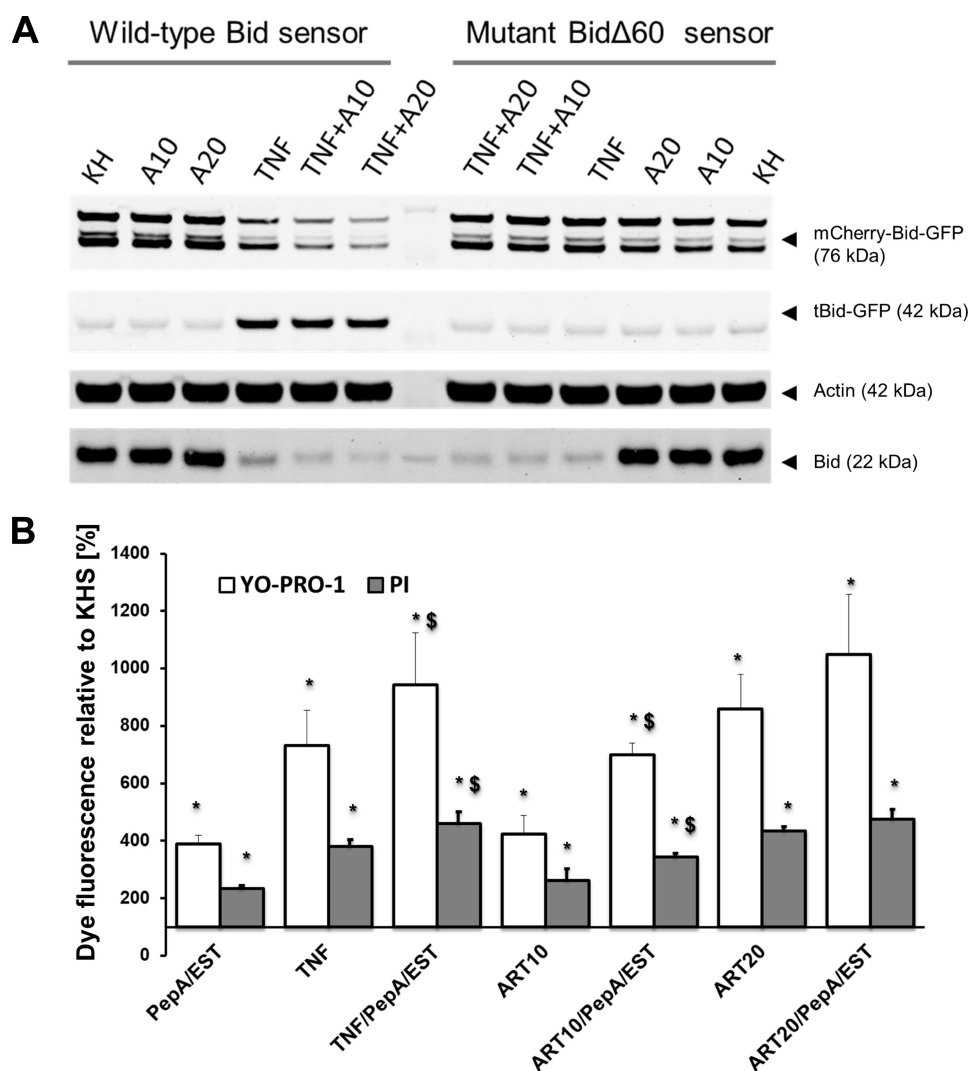


FIGURE 8. ART alone does not cause Bid cleavage but can amplify TNF-induced Bid cleavage. *A*, Western blot detection of Bid activity in response to ART is shown. Stable cell lines expressing either a wild-type Bid sensor (mCherry-Bid-GFP) or a caspase 8-insensitive Bid Δ 60 sensor were treated with TNF, ART, or combined TNF/ART. tBid-GFP was detected using antibody against GFP. Endogenous Bid was detected using antibody against Bid. *B*, wild-type MCF-7 cells were subjected to 48 h of treatment with or without cathepsin inhibitors PepA (5 μ M) and EST (10 μ M). Graphs indicate responses as the percentage of dye fluorescence normalized to KHS, and the x axis crosses at 100%, i.e. basal KHS levels (*, $p < 0.05$, compared with KHS control; \$, $p < 0.05$, with PepA/EST versus without PepA/EST).

In non-tumorigenic MCF-10A cells, none of the treatments induced appreciable cell death. As a positive control for cell death, MCF-10A cells were treated with TNF combined with MG132 (10 μ M) to block TNF pro-survival signaling (54), which resulted in significant cell death (Fig. 9*Aii*).

Next, we investigated the impact of ART on lysosomal localization and mitochondrial fragmentation (Fig. 9*B*), both characteristic parameters of the PCD pathway described above. Similar to MCF-7 cells, in T47D and MDA-MB-231 cells ART induced clustering of Lamp2a-stained lysosomes to perinuclear regions (data not shown). This effect was more

pronounced in cells co-treated with ART and HTF and was reversible by DFO. In both T47D and MDA-MB-231 cells, mitochondrial networks fragmented in a lysosomal iron-dependent manner and mitochondria remained unclustered. In contrast, lysosomal distribution and mitochondrial morphology remained unaltered in MCF-10A cells treated either with ART alone or in combination with HTF.

DISCUSSION

Our results demonstrate that in breast cancer cells ART exerts multifarious effects on protein, second messengers, and

FIGURE 7. ART activates mitochondrial apoptosis that is dependent on lysosomal iron. *A*, the impact of ART on mitochondrial morphology was investigated in MCF-7 cells stably expressing the outer mitochondrial membrane GFP marker at 24 h of drug treatment. *B*, MCF-7 cells stably expressing GFP-Bax were incubated in either KHS alone or in combination with the indicated drugs for 24 h. *Bi*, shown are representative maximum Z-projections. *Bii*, quantification was performed by classifying GFP-Bax cells as displaying either diffuse cytosolic or clustered mitochondrial GFP-Bax. Represented is the percentage of cells with punctate GFP-Bax distribution (*, $p < 0.05$, compared with KHS; \$, $p < 0.05$, without DFO versus with DFO). *C*, cytochrome *c* release was quantified in wild-type MCF-7 cells by classifying mitochondrial cytochrome *c*, i.e. colocalized cytochrome *c* and COX IV, or released cytochrome *c*, i.e. little or no colocalization of cytochrome *c* with COX IV. Represented is the percentage of cells with released cytochrome *c* per total cells scored (*, $p < 0.05$; #, $p < 0.001$, compared with KHS; \$, $p < 0.05$, without DFO versus with DFO).

Artesunate Triggers Lysosomal Cell Death

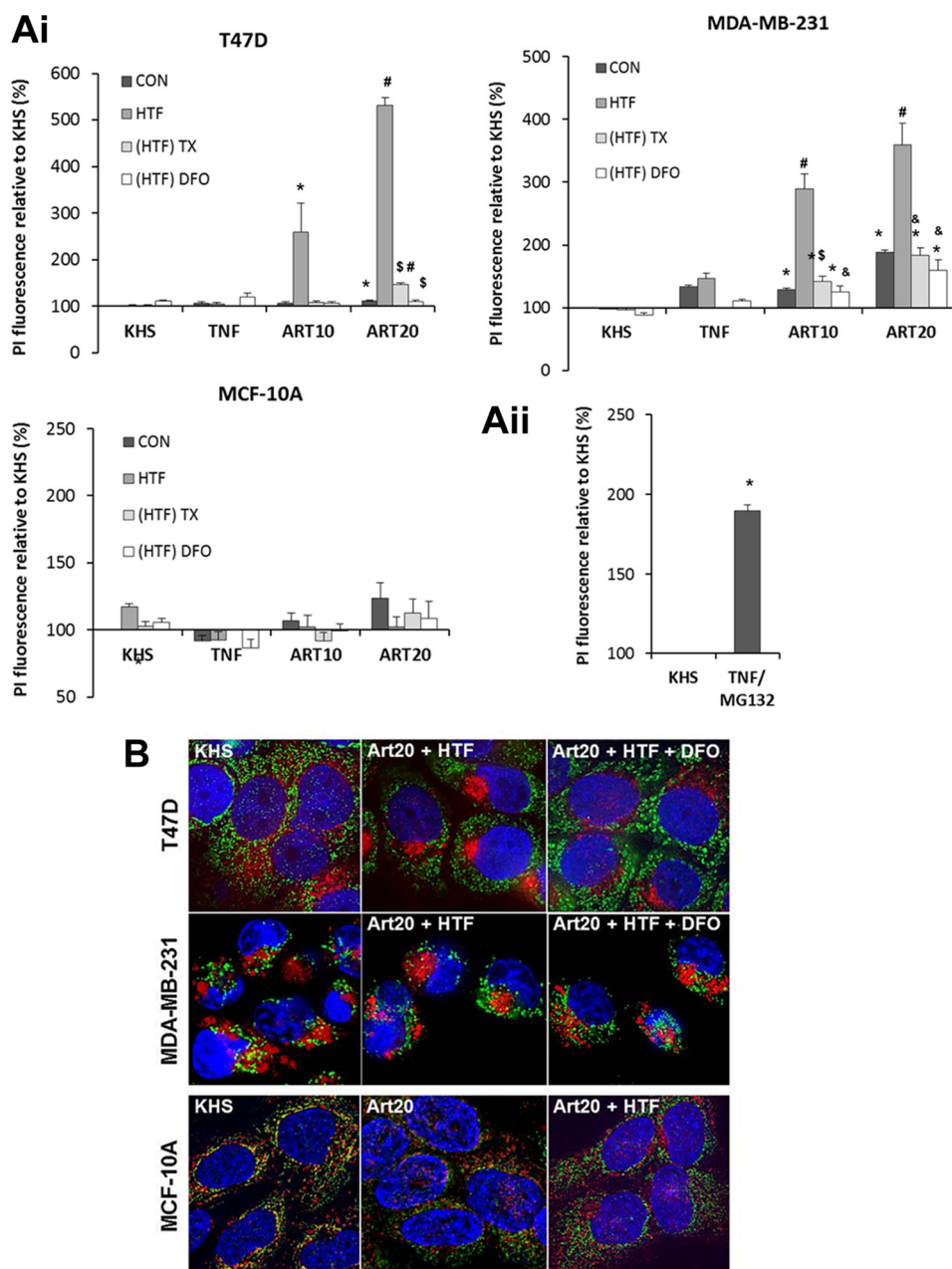


FIGURE 9. T47D and MDA-MB-231 but not MCF-10A cells undergo lysosomal PCD upon ART treatment. *Ai*, T47D, MDA-MB-231, and MCF-10A cells were treated for 48 h with 10 or 20 $\mu\text{g}/\text{ml}$ ART in KHS in combination with the indicated co-treatments. The KHS data set contains single treatments with TX, DFO, or HTF. In ART10 and ART20 data sets, TX and DFO were added in co-treatment with HTF, as ART10 and ART20 alone had a minor effect on cell death. Cell death was measured using PI staining. Represented is the percentage of dye fluorescence normalized to KHS, and the x axis crosses at 100% (basal KHS levels) (*, $p < 0.05$; #, $p < 0.001$, compared with KHS control; &, $p < 0.05$; \$, $p < 0.001$, ART + HTF without versus with co-treatment with DFO or TX). *Aii*, as a positive control for death induction, MCF-10A cells were treated with KHS with and without TNF in combination with 10 μM MG132 for 24 h. Cell death was determined as in *Ai* (*, $p < 0.05$, compared with KHS). *B*, T47D, MDA-MB-231, and MCF-10A cells were treated with the indicated drug combinations. At 24 h cells were fixed and immunostained for COX IV and Lamp2a to assess the intracellular localization of mitochondria (green) and lysosomes (red), respectively. Nuclei were stained with Hoechst 33342 (blue).

organelles involved in PCD signaling. Lysosomes were identified as the primary target of ART, being converted to pro-death organelles through iron-catalyzed generation of ROS. Downstream of lysosomal ROS production, mitochondrial apoptotic cell death was activated. Additionally, ART globally disrupted the endolysosomal trafficking and inhibited autophagic flux.

Lysosomes and Mitochondrial Apoptosis—TNF was utilized here as an established initiator of mitochondrial apoptosis

(50) and, presumably, lysosomal dysfunction through ceramide production and cathepsin release (46, 55, 56). TNF activated mitochondrial apoptosis, evidenced by prominent mitochondrial fragmentation, Bax activation, and cytochrome *c* release concomitant with death. Although no impact was detected on functional parameters or localization of the endolysosomal pathway, the suppressive effect of TNF on autophagy, *i.e.* increased steady-state levels of LC3B-I and LC3-II, indicates uncoupling of lysosomes from autophagosomes.

ART killing mechanisms differed significantly from TNF signaling. ROS were determined as causative in ART-triggered cell death (Fig. 1B) in agreement with previous findings (10, 12). Here, we identified lysosomal iron as the lethal source of ART-generated ROS; the lysosomal iron chelator DFO blocked both ROS production (Fig. 2A) and disruption to endolysosomal trafficking (Figs. 5 and 9B), inhibited several parameters associated with MOMP (Figs. 7 and 9B), and protected against ART-induced cell death (Figs. 2B and 9Ai). Conversely, enhancing free lysosomal iron by the addition of HTF enhanced ART killing in a cell line-dependent manner (Figs. 2C and 9Ai). Thus, although basal lysosomal iron content in both estrogen receptor-positive and -negative breast cancer cells is sufficient to enable ART toxicity, it represents a targetable limiting factor in ART killing potential in cancer cells. Indeed, iron supplementation enhanced ART killing in different cancer cells (14, 57), and ART toxicity is positively correlated with expression of proteins involved in iron metabolism (58).

These findings may offer insight into the high killing specificity of ART in cancer cells (59). Notably, we show that non-transformed MCF-10A cells were highly resistant to ART and ART/HTF. Because of an iron dependence for enhanced proliferation (60), lysosomes of cancer cells contain higher levels of redox active iron and consequently may be more susceptible to ROS-mediated membrane destabilization (61).

Lysosomal membrane permeabilization-triggered mitochondrial apoptosis (45, 46, 48, 62) requires cytosolic release of cathepsins to activate MOMP (46, 63). Here, however, lysosomal inhibitors enhanced TNF killing (Fig. 8B), suggesting a signal attenuation role for the lysosome in death receptor signaling analogous to lysosomal control of EGF receptor activity (64) and indicating that in MCF-7 cells, under the conditions used here, lysosomal membrane permeabilization was not a component of TNF receptor signaling. Importantly, as TNF is a potent endogenous cytokine present in the tumor environment and ART amplified the activation of pro-apoptotic Bid by TNF, our data suggest a potential of ART to amplify the innate cell killing potential. Through the use of a Bid mutant for the major caspase 8 cleavage site, we implicate either caspase 2 and/or caspase 8, which cleave at Asp-60 (50), as the major proteolytic pathway amplified by ART. As cathepsin inhibitors did not protect against cell death (Fig. 8) and ART alone did not activate Bid cleavage, ART-induced lysosomal death signaling is mechanistically distinct from previous reports of lysosome-to-mitochondria apoptotic signaling. Moreover, different modes of lysosomal functional disruption via co-treatment with CQ, which enhanced lysosomal pH and cathepsin activity (Fig. 5C), or BAF, which decreased lysosomal pH and cathepsin activity, resulted in a reduction of ART-induced cell death, indicating that a functional lysosomal compartment is required for ART killing. These findings are relevant when considering co-treatment strategies, as one might assume that additional targeting of lysosomes would enhance ART-induced PCD.

Notably, ART induced iron-dependent vesicle clustering to the perinuclear region. In MCF-7 cells, autophagosomes (LC3B-positive) and early (Rab5-positive) and late (Rab7-pos-

itive) endosomes were all found in perinuclear clusters (Figs. 3A and 4). The same effect was observed for lysosomes (Lamp2a-positive) in T47D and MDA-MB-231 cells (Fig. 9B). Remarkably, non-transformed MCF-10A cells, which were resistant to ART-induced cell death, did not show clustering of Lamp2a-positive lysosomes (Fig. 9B). The clustering effect was specific, as mitochondria that had fragmented in response to ART were symmetrically dispersed (Figs. 7A and 9B). As indicated by LTR and MR staining, clustered lysosomes retained activity (Fig. 5B), and as microtubules remained stabilized (results not shown), we hypothesized that ART-induced oxidative stress targets motor proteins and/or adaptors that link autophagosomal, lysosomal, and endocytic vesicles to the cytoskeleton (65, 66).

Clustering of the autophagosomal and endolysosomal compartments may broadly impact cell physiology. Strikingly, ART was found to disrupt autophagic flux (Fig. 4), *i.e.* ART treatment resulted in the accumulation of steady-state AVs, whereas total AV formation (seen as cumulative AVs under BAF co-treatment) remained unaltered. Thus, although AVs and lysosomes were clustered in the same perinuclear region, ART blocked AV degradation, presumably because of either impaired fusion with lysosomes and/or reduced lysosomal degradative activity. It is conceivable that the ART-induced disruption to autophagy counteracts pro-survival roles of autophagy such as the recycling of macromolecules. Furthermore, as scavenging of pro-apoptotic mitochondria is cytoprotective (34), the spatial uncoupling of autophagy and mitochondria may play a role in ART toxicity. Moreover, cathepsins released from cancer cells participate in the degradation of the extracellular matrix to promote tumor cell migration and angiogenesis (67). Clustering of lysosomes can limit invasiveness (68) and may be a possible mechanism by which ART reduces cell migration and invasion (69). Similarly, clustering of Rab5-labeled vesicles, which participate in both autophagy (70) and endocytosis (70), may alter the endocytic capacity of the cell. Such decoupling among receptor internalization, trafficking, and degradation may contribute to ART amplification of caspase activation by TNF, a relevant cytokine in the tumor microenvironment.

Relevance of Artemisinin and Its Derivatives—ART and its derivatives induce PCD in cancer cell culture systems, including colon, breast, ovarian, prostate (59), pancreatic (71), and leukemia (12) cell lines. *In vivo*, artemisinin and its derivatives have shown promising anti-tumor effects against Kaposi sarcoma (7), pancreatic cancer (5), and hepatomas (6) in mouse xenograft models. Importantly, the pharmacokinetics and tolerance of ART as an anti-malarial agent are well documented (72), and it is currently in clinical trial as a treatment against breast cancer (ClinicalTrials.gov ID: NCT00764036). To date, the focus has been on its activation of ROS-mediated induction of mitochondrial apoptosis and inhibition of pro-survival signaling, including NF κ B and receptor tyrosine kinase pathways (73, 74), and DNA damage (75). Lysosomes provide a cancer-enriched target that activates alternative modes of PCD (76). Lysosomotropic agents such as chloroquine can be used as selective killing tools against cancer cells both in cell culture (45) and *in vivo* (77). Our work identifies

Artesunate Triggers Lysosomal Cell Death

ART as a novel tool to specifically induce lysosomal PCD in breast cancer cells while having little effect on non-transformed breast epithelial cells. ART-induced lysosomal PCD involves disrupted endolysosomal trafficking, blocked autophagy, and enhanced ROS production upstream of mitochondrial apoptosis. *In vivo* experiments will now be required to determine to what extent iron supplementation is an effective means of enhancing the specificity of ART action in cancer cells and whether ART can enhance the endogenous innate immune response, e.g. TNF-mediated mitochondrial apoptosis, as well as separate reported anti-angiogenic, signaling, and apoptotic effects from non-canonical PCD.

Acknowledgments—We gratefully acknowledge the kind gift of GFP-Rab7 from Prof. B. van Deurs (Copenhagen University), mitoNEET-(1–23)-GFP from Prof. J. Dixon (University of California, San Diego), pRSET-mCherry from Prof. R. Tsien (University of California, San Diego), GFP-LC3 from Prof. T. Yoshimori (Osaka University), and GFP-Bax from Prof. R. Youle (National Institutes of Health).

REFERENCES

1. Klayman, D. L. (1985) *Science* **228**, 1049–1055
2. Efferth, T., and Volm, M. (2005) *In Vivo* **19**, 225–232
3. Lai, H., Sasaki, T., Singh, N. P., and Messay, A. (2005) *Life Sci.* **76**, 1267–1279
4. Efferth, T. (2006) *Curr. Drug Targets* **7**, 407–421
5. Chen, H., Sun, B., Pan, S., Jiang, H., and Sun, X. (2009) *Anticancer Drugs* **20**, 131–140
6. Hou, J., Wang, D., Zhang, R., and Wang, H. (2008) *Clin. Cancer Res.* **14**, 5519–5530
7. Dell'Eva, R., Pfeffer, U., Vené, R., Anfosso, L., Forlani, A., Albin, A., and Efferth, T. (2004) *Biochem. Pharmacol.* **68**, 2359–2366
8. Taylor, W. R., and White, N. J. (2004) *Drug Saf.* **27**, 25–61
9. Berger, T. G., Dieckmann, D., Efferth, T., Schultz, E. S., Funk, J. O., Baur, A., and Schuler, G. (2005) *Oncol. Rep.* **14**, 1599–1603
10. Efferth, T., Sauerbrey, A., Olbrich, A., Gebhart, E., Rauch, P., Weber, H. O., Hengstler, J. G., Halatsch, M. E., Volm, M., Tew, K. D., Ross, D. D., and Funk, J. O. (2003) *Mol. Pharmacol.* **64**, 382–394
11. Wu, G. D., Zhou, H. J., and Wu, X. H. (2004) *Vascul. Pharmacol.* **41**, 205–212
12. Efferth, T., Giaisi, M., Merling, A., Krammer, P. H., and Li-Weber, M. (2007) *PLoS One* **2**, e693
13. Singh, N. P., and Lai, H. (2001) *Life Sci.* **70**, 49–56
14. Efferth, T., Benakis, A., Romero, M. R., Tomicic, M., Rauh, R., Steinbach, D., Häfer, R., Stamminger, T., Oesch, F., Kaina, B., and Marschall, M. (2004) *Free Radic. Biol. Med.* **37**, 998–1009
15. Pandey, A. V., Tekwani, B. L., Singh, R. L., and Chauhan, V. S. (1999) *J. Biol. Chem.* **274**, 19383–19388
16. Mizushima, N. (2007) *Genes Dev.* **21**, 2861–2873
17. Bridges, K. R. (1987) *J. Biol. Chem.* **262**, 14773–14778
18. Kurz, T., Terman, A., Gustafsson, B., and Brunk, U. T. (2008) *Histochem. Cell Biol.* **129**, 389–406
19. Uchiyama, A., Kim, J. S., Kon, K., Jaeschke, H., Ikejima, K., Watanabe, S., and Lemasters, J. J. (2008) *Hepatology* **48**, 1644–1654
20. Kurz, T., Terman, A., and Brunk, U. T. (2007) *Arch. Biochem. Biophys.* **462**, 220–230
21. Boya, P., and Kroemer, G. (2008) *Oncogene* **27**, 6434–6451
22. Blomgran, R., Zheng, L., and Stendahl, O. (2007) *J. Leukoc. Biol.* **81**, 1213–1223
23. Droga-Mazovec, G., Bojic, L., Petelin, A., Ivanova, S., Romih, R., Repnik, U., Salvesen, G. S., Stoka, V., Turk, V., and Turk, B. (2008) *J. Biol. Chem.* **283**, 19140–19150
24. Conus, S., Perozzo, R., Reinheckel, T., Peters, C., Scapozza, L., Yousefi, S., and Simon, H. U. (2008) *J. Exp. Med.* **205**, 685–698
25. Kabeya, Y., Mizushima, N., Ueno, T., Yamamoto, A., Kirisako, T., Noda, T., Kominami, E., Ohsumi, Y., and Yoshimori, T. (2000) *EMBO J.* **19**, 5720–5728
26. Ortiz-Ferrón, G., Tait, S. W., Robledo, G., de Vries, E., Borst, J., and López-Rivas, A. (2006) *Cell Death Differ.* **13**, 1857–1865
27. Li, H., Zhu, H., Xu, C. J., and Yuan, J. (1998) *Cell* **94**, 491–501
28. Wiley, S. E., Murphy, A. N., Ross, S. A., van der Geer, P., and Dixon, J. E. (2007) *Proc. Natl. Acad. Sci. U.S.A.* **104**, 5318–5323
29. Wolter, K. G., Hsu, Y. T., Smith, C. L., Nechushtan, A., Xi, X. G., and Youle, R. J. (1997) *J. Cell Biol.* **139**, 1281–1292
30. Bucci, C., Thomsen, P., Nicoziani, P., McCarthy, J., and van Deurs, B. (2000) *Mol. Biol. Cell* **11**, 467–480
31. Plantin-Carrenard, E., Bringuier, A., Derappe, C., Pichon, J., Guillot, R., Bernard, M., Foglietti, M. J., Feldmann, G., Aubery, M., and Braut-Boucher, F. (2003) *Cell Biol. Toxicol.* **19**, 121–133
32. Swift, L. M., and Sarvazyan, N. (2000) *Am. J. Physiol. Heart Circ. Physiol.* **278**, H982–H990
33. Jäger, S., Bucci, C., Tanida, I., Ueno, T., Kominami, E., Saftig, P., and Eskelinen, E. L. (2004) *J. Cell Sci.* **117**, 4837–4848
34. Hamacher-Brady, A., Brady, N. R., Logue, S. E., Sayen, M. R., Jinno, M., Kirshenbaum, L. A., Gottlieb, R. A., and Gustafsson, A. B. (2007) *Cell Death Differ.* **14**, 146–157
35. Efferth, T., Briehl, M. M., and Tome, M. E. (2003) *Int. J. Oncol.* **23**, 1231–1235
36. Miura, T., Muraoka, S., and Ogiso, T. (1993) *Biochem. Mol. Biol. Int.* **31**, 125–133
37. Cable, H., and Lloyd, J. B. (1999) *J. Pharm. Pharmacol.* **51**, 131–134
38. Hamacher-Brady, A., Brady, N. R., and Gottlieb, R. A. (2006) *J. Biol. Chem.* **281**, 29776–29787
39. Klionsky, D. J., Abeliovich, H., Agostinis, P., Agrawal, D. K., Aliev, G., Askew, D. S., Baba, M., Baehrecke, E. H., Bahr, B. A., Ballabio, A., Bamber, B. A., Bassham, D. C., Bergamini, E., Bi, X., Biard-Piechaczyk, M., Blum, J. S., Bredesen, D. E., Brodsky, J. L., Brumell, J. H., Brunk, U. T., Bursch, W., Camougrand, N., Cebollero, E., Cecconi, F., Chen, Y., Chin, L. S., Choi, A., Chu, C. T., Chung, J., Clarke, P. G., Clark, R. S., Clarke, S. G., Clavé, C., Cleveland, J. L., Codogno, P., Colombo, M. I., Coto-Montes, A., Cregg, J. M., Cuervo, A. M., Debnath, J., Demarchi, F., Dennis, P. B., Dennis, P. A., Deretic, V., Devenish, R. J., Di Sano, F., Dice, J. F., Difiglia, M., Dinesh-Kumar, S., Distelhorst, C. W., Djavaheri-Mergny, M., Dorsey, F. C., Dröge, W., Dron, M., Dunn, W. A., Jr., Duszenko, M., Eissa, N. T., Elazar, Z., Esclatine, A., Eskelinen, E. L., Fésüs, L., Finley, K. D., Fuentes, J. M., Fucyo, J., Fujisaki, K., Galloti, B., Gao, F. B., Gewirtz, D. A., Gibson, S. B., Gohla, A., Goldberg, A. L., Gonzalez, R., González-Estévez, C., Gorski, S., Gottlieb, R. A., Häusser, D., He, Y. W., Heidenreich, K., Hill, J. A., Hoyer-Hansen, M., Hu, X., Huang, W. P., Iwasaki, A., Jäättelä, M., Jackson, W. T., Jiang, X., Jin, S., Johansen, T., Jung, J. U., Kadowaki, M., Kang, C., Kelekar, A., Kessel, D. H., Kiel, J. A., Kim, H. P., Kimchi, A., Kinsella, T. J., Kiselyov, K., Kitamoto, K., Knecht, E., Komatsu, M., Kominami, E., Kondo, S., Kovács, A. L., Kroemer, G., Kuan, C. Y., Kumar, R., Kundu, M., Landry, J., Laporte, M., Le, W., Lei, H. Y., Lenardo, M. J., Levine, B., Lieberman, A., Lim, K. L., Lin, F. C., Liou, W., Liu, L. F., Lopez-Berestein, G., López-Otín, C., Lu, B., Macleod, K. F., Malorni, W., Martinet, W., Matsuoka, K., Mautner, J., Meijer, A. J., Melendez, A., Michels, P., Miotto, G., Mistiaen, W. P., Mizushima, N., Mograbi, B., Monastyrski, I., Moore, M. N., Moreira, P. I., Moriyasu, Y., Motyl, T., Munz, C., Murphy, L. O., Naqvi, N. I., Neufeld, T. P., Nishino, I., Nixon, R. A., Noda, T., Nurnberg, B., Ogawa, M., Oleinick, N. L., Olsen, L. J., Ozpolat, B., Paglin, S., Palmer, G. E., Papassideri, I., Parkes, M., Perlmutter, D. H., Perry, G., Piacentini, M., Pinkas-Kramarski, R., Prescott, M., Proikas-Cezanne, T., Raben, N., Rami, A., Reggiori, F., Rohrer, B., Rubinsztein, D. C., Ryan, K. M., Sadoshima, J., Sakagami, H., Sakai, Y., Sandri, M., Sasakawa, C., Sass, M., Schneider, C., Seglen, P. O., Selverstov, O., Settleman, J., Shacka, J. J., Shapiro, I. M., Sibirny, A., Silva-Zacarin, E. C., Simon, H. U., Simone, C., Simonsen, A., Smith, M. A., Spaniel-Borowski, K., Srinivas, V., Steeves, M., Stenmark, H., Stromhaug, P. E., Subauste, C. S., Sugimoto, S., Sulzer, D., Suzuki, T., Swanson, M. S., Tabas, I., Takeshita, F., Talbot, N. J., Talloczy, Z., Tanaka, K., Tanaka, K., Tanida, I., Taylor, G. S., Taylor, J. P.,

- Terman, A., Tettamanti, G., Thompson, C. B., Thumm, M., Tolkovsky, A. M., Tooze, S. A., Truant, R., Tumanovska, L. V., Uchiyama, Y., Ueno, T., Uzcátegui, N. L., van der Klei, I., Vaquero, E. C., Vellai, T., Vogel, M. W., Wang, H. G., Webster, P., Wiley, J. W., Xi, Z., Xiao, G., Yahalom, J., Yang, J. M., Yap, G., Yin, X. M., Yoshimori, T., Yu, L., Yue, Z., Yuzaki, M., Zabinryk, O., Zheng, X., Zhu, X., and Deter, R. L. (2008) *Autophagy* **4**, 151–175
40. Yoshimori, T., Yamamoto, A., Moriyama, Y., Futai, M., and Tashiro, Y. (1991) *J. Biol. Chem.* **266**, 17707–17712
41. Simonsen, A., and Tooze, S. A. (2009) *J. Cell Biol.* **186**, 773–782
42. Zerial, M., and McBride, H. (2001) *Nat. Rev. Mol. Cell Biol.* **2**, 107–117
43. Stenmark, H., Parton, R. G., Steele-Mortimer, O., Lütcke, A., Gruenberg, J., and Zerial, M. (1994) *EMBO J.* **13**, 1287–1296
44. Shacka, J. J., Klocke, B. J., Shibata, M., Uchiyama, Y., Datta, G., Schmidt, R. E., and Roth, K. A. (2006) *Mol. Pharmacol.* **69**, 1125–1136
45. Boya, P., Gonzalez-Polo, R. A., Poncet, D., Andreau, K., Vieira, H. L., Roumier, T., Perfettini, J. L., and Kroemer, G. (2003) *Oncogene* **22**, 3927–3936
46. Guicciardi, M. E., Deussing, J., Miyoshi, H., Bronk, S. F., Svingen, P. A., Peters, C., Kaufmann, S. H., and Gores, G. J. (2000) *J. Clin. Invest.* **106**, 1127–1137
47. Suen, D. F., Norris, K. L., and Youle, R. J. (2008) *Genes Dev.* **22**, 1577–1590
48. Werneburg, N. W., Guicciardi, M. E., Bronk, S. F., Kaufmann, S. H., and Gores, G. J. (2007) *J. Biol. Chem.* **282**, 28960–28970
49. Brady, N. R., Hamacher-Brady, A., and Gottlieb, R. A. (2006) *Biochim. Biophys. Acta* **1757**, 667–678
50. Luo, X., Budihardjo, I., Zou, H., Slaughter, C., and Wang, X. (1998) *Cell* **94**, 481–490
51. Yin, X. M. (2006) *Gene* **369**, 7–19
52. Lu, M., Mira-y-Lopez, R., Nakajo, S., Nakaya, K., and Jing, Y. (2005) *Oncogene* **24**, 4362–4369
53. Yang, S., Liu, J., Thor, A. D., and Yang, X. (2007) *Oncol. Rep.* **17**, 1229–1235
54. Palombella, V. J., Rando, O. J., Goldberg, A. L., and Maniatis, T. (1994) *Cell* **78**, 773–785
55. Werneburg, N. W., Guicciardi, M. E., Bronk, S. F., and Gores, G. J. (2002) *Am. J. Physiol. Gastrointest. Liver Physiol.* **283**, G947–G956
56. Werneburg, N., Guicciardi, M. E., Yin, X. M., and Gores, G. J. (2004) *Am. J. Physiol. Gastrointest. Liver Physiol.* **287**, G436–G443
57. Woerdenbag, H. J., Moskal, T. A., Pras, N., Malingré, T. M., el-Feraly, F. S., Kampinga, H. H., and Konings, A. W. (1993) *J. Nat. Prod.* **56**, 849–856
58. Kelter, G., Steinbach, D., Konkimalla, V. B., Tahara, T., Taketani, S., Fiebig, H. H., and Efferth, T. (2007) *PLoS One* **2**, e798
59. Efferth, T., Dunstan, H., Sauerbrey, A., Miyachi, H., and Chitambar, C. R. (2001) *Int. J. Oncol.* **18**, 767–773
60. Yu, Y., Kovacevic, Z., and Richardson, D. R. (2007) *Cell Cycle* **6**, 1982–1994
61. Kroemer, G., and Jäättelä, M. (2005) *Nat. Rev. Cancer* **5**, 886–897
62. Boya, P., Andreau, K., Poncet, D., Zamzami, N., Perfettini, J. L., Metivier, D., Ojcius, D. M., Jäättelä, M., and Kroemer, G. (2003) *J. Exp. Med.* **197**, 1323–1334
63. Cirman, T., Oresiaë, K., Mazovec, G. D., Turk, V., Reed, J. C., Myers, R. M., Salvesen, G. S., and Turk, B. (2004) *J. Biol. Chem.* **279**, 3578–3587
64. Dikic, I. (2003) *Biochem. Soc. Trans.* **31**, 1178–1181
65. Brown, C. L., Maier, K. C., Stauber, T., Ginkel, L. M., Wordeman, L., Vernos, I., and Schroer, T. A. (2005) *Traffic* **6**, 1114–1124
66. Jahreiss, L., Menzies, F. M., and Rubinsztein, D. C. (2008) *Traffic* **9**, 574–587
67. Vasiljeva, O., and Turk, B. (2008) *Biochimie* **90**, 380–386
68. Steffan, J. J., Williams, B. C., Welbourne, T., and Cardelli, J. A. (2010) *J. Cell Sci.* **123**, 1151–1159
69. Rasheed, S. A., Efferth, T., Asangani, I. A., and Allgayer, H. (2010) *Int. J. Cancer* **127**, 1475–1485
70. Ravikumar, B., Imarisio, S., Sarkar, S., O’Kane, C. J., and Rubinsztein, D. C. (2008) *J. Cell Sci.* **121**, 1649–1660
71. Youns, M., Efferth, T., Reichling, J., Fellenberg, K., Bauer, A., and Hoheisel, J. D. (2009) *Biochem. Pharmacol.* **78**, 273–283
72. Orrell, C., Little, F., Smith, P., Folb, P., Taylor, W., Olliaro, P., and Barnes, K. I. (2008) *Eur. J. Clin. Pharmacol.* **64**, 683–690
73. Xu, H., He, Y., Yang, X., Liang, L., Zhan, Z., Ye, Y., Yang, X., Lian, F., and Sun, L. (2007) *Rheumatology* **46**, 920–926
74. Konkimalla, V. B., McCubrey, J. A., and Efferth, T. (2009) *Curr. Cancer Drug Targets* **9**, 72–80
75. Li, P. C., Lam, E., Roos, W. P., Zdzienicka, M. Z., Kaina, B., and Efferth, T. (2008) *Cancer Res.* **68**, 4347–4351
76. Kirkegaard, T., and Jäättelä, M. (2009) *Biochim. Biophys. Acta* **1793**, 746–754
77. Maclean, K. H., Dorsey, F. C., Cleveland, J. L., and Kastan, M. B. (2008) *J. Clin. Invest.* **118**, 79–88